

Sparse Range-constrained Learning and Its Application for Medical Image Grading

Jun Cheng

Abstract—Sparse learning has been shown to be effective in solving many real-world problems. Finding sparse representations is a fundamentally important topic in many fields of science including signal processing, computer vision, genome study and medical imaging. One important issue in applying sparse representation is to find the basis to represent the data, especially in computer vision and medical imaging where the data is not necessary incoherent. In medical imaging, clinicians often grade the severity or measure the risk score of a disease based on images. This process is referred to as medical image grading. Manual grading of the disease severity or risk score is often used. However, it is tedious, subjective and expensive. Sparse learning has been used for automatic grading of medical images for different diseases. In the grading, we usually begin with one step to find a sparse representation of the testing image using a set of reference images or atoms from the dictionary. Then in the second step, the selected atoms are used as references to compute the grades of the testing images. Since the two steps are conducted sequentially, the objective function in the first step is not necessarily optimized for the second step. In this paper, we propose a novel sparse range-constrained learning (SRCL) algorithm for medical image grading. Different from most of existing sparse learning algorithms, SRCL integrates the objective of finding a sparse representation and that of grading the image into one function. It aims to find a sparse representation of the testing image based on atoms that are most similar in both the data or feature representation and the medical grading scores. We apply the new proposed SRCL to two different applications, namely, cup-to-disc ratio computation from retinal fundus images and cataract grading from slit-lamp lens images. Experimental results show that the proposed method is able to improve the accuracy in cup-to-disc ratio computation and cataract grading.

Index Terms- sparse learning, medical image analysis, computer aided diagnosis

I. INTRODUCTION

Sparse learning is a representation learning method which aims at finding a sparse representation of the input data in the form of a linear combination of basic elements as well as those basic elements themselves. These elements are called atoms and they form a dictionary. Atoms in the dictionary are not necessarily orthogonal, and they may be in an over-complete spanning set. Sparse learning has been shown to be effective in solving many real-world problems. Finding sparse representations is a fundamentally important topic in many fields of science including signal processing, computer vision, genome study and medical imaging. In audio processing,

This work was supported in part by Cixi Institute of Biomedical Engineering, Chinese Academy of Sciences, China, under Grant Y80002RA01. (Corresponding Author Jun Cheng)

J. Cheng is with Cixi Institute of Biomedical Engineering, Chinese Academy of Sciences, China (email: chengjun@nimte.ac.cn).

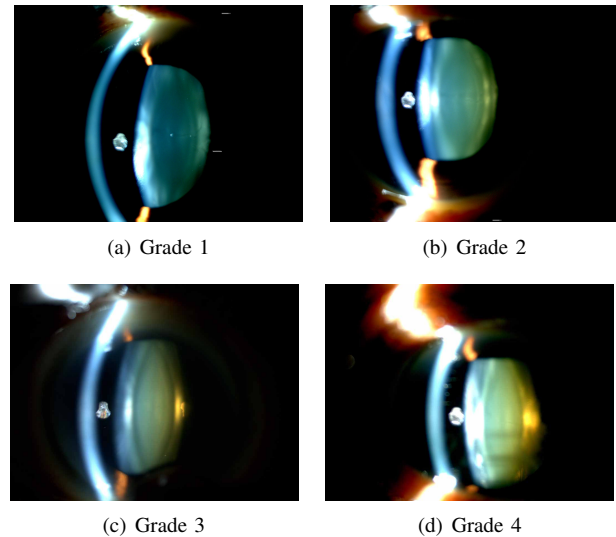


Fig. 1. Four slit-lamp images with manual grading from 1 to 4.

sparse representation was used to decompose sounds in terms of a dictionary of Gammatone functions [1]. In [2], it was also used for blind source separation and EEG signal analysis. In image processing, sparsity has been shown to be promising in denoising and enhancement [3]–[10]. In computer vision tasks such as face recognition [11]–[14], sparsity has been widely used as well. In genome-wide association studies, only a small portion of genes has been found to contribute to different diseases [15]–[17]. In medical imaging, sparse learning based approaches have been used for brain image analysis [18]–[20]. Recently, sparsity has been used for medical image grading [21], [22].

Clinicians often grade the severity or measure the risk score of a disease based on images. This process is referred to as medical image grading. Very often, the image to be graded is compared with some reference images based on protocols. For example, four standard images with grade 1 to 4, similar to that in Fig. 1, are provided as reference images in cataract grading [21]. Clinicians often compare a new image with the standard images to get a decimal grading score. In diabetic retinopathy grading, the clinicians examine the retinal images to determine the presence and types of lesions, which would be used to determine the severity or stage of the diseases. In glaucoma diagnosis, the clinicians measure the vertical cup-to-disc ratio (CDR) as a risk factor for glaucoma. However, manual assessment or grading of the images is subjective, time-consuming and expensive. Therefore, automatic grading

of the images is expected to improve the clinical management of the diseases and provide an objective assessment for studies.

Inspired by the manual grading process by clinicians, sparse learning has been proposed for medical image grading. Let $X = [\mathbf{x}_1, \mathbf{x}_2, \dots, \mathbf{x}_n] \in \mathbb{R}^{m \times n}$ be a matrix or a dictionary consists of n known samples or atoms and $\mathbf{y} \in \mathbb{R}^m$ is a sample to be represented, m denotes the number of features to represent each sample. We want to use X to represent \mathbf{y} as:

$$\hat{\mathbf{y}} = X\mathbf{w}, \quad (1)$$

where $\mathbf{w} = [w_1, w_2, \dots, w_n]^T \in \mathbb{R}^n$. In sparse learning, we want to obtain a solution of \mathbf{w} with majority of elements to be zero or close to zero. A typical form of the objective function for sparse learning is given as:

$$\min_{\mathbf{w}} f(X, \mathbf{y}, \mathbf{w}) + \lambda \cdot \|\mathbf{w}\|_0. \quad (2)$$

Very often, the first term, also called the data term, is computed as

$$f(X, \mathbf{y}, \mathbf{w}) = \|\mathbf{y} - X\mathbf{w}\|_2^2 \quad (3)$$

In the data term, \mathbf{y} and X can be the original pixel intensities or features computed from the pixel intensities. The second term is the regularization term to ensure the sparsity and λ controls the weight of the term. Because of the ℓ_0 norm term, the minimization problem above is not convex and the solving of problem is NP-hard [23]. Very often, ℓ_1 norm is used instead to ensure sparsity and convert the problem to a convex optimization problem [24].

One important issue in computing the sparse representation is to choose the atoms to represent the data [25]. In another word, how to determine the non-zero elements and their corresponding weights in \mathbf{w} . In signal processing, the performances of sparse approximation algorithms often depend on the mutual coherence of the data in the dictionary and much effort has been given to learn from incoherent dictionary [26]. In computer vision, we often have to learn from overcomplete dictionary where the data is not necessarily incoherent as well.

In the past, different variations and extensions of sparse learning algorithms have been proposed, including ℓ_1 norm, ℓ_1/ℓ_q norm [27], fused lasso [28], locality-constrained linear coding [29], Laplacian sparse coding [30], similarity weighted sparse representation [31], sparse dissimilarity-constrained coding [22], sparse group lasso [32], tree structured group lasso [33], overlapping group lasso [34], ordered tree-nonnegative max-heap [35], and trace-norm [36]. The objective functions of these different sparse models can be generally summarized as:

$$\min_{\mathbf{w}} f(X, \mathbf{y}, \mathbf{w}) + \lambda \cdot r(\mathbf{w}), \quad (4)$$

where $r(\mathbf{w})$ is a function of \mathbf{w} only, such as ℓ_1 norm $r(\mathbf{w}) = \|\mathbf{w}\|_1$, ℓ_2 norm $r(\mathbf{w}) = \|\mathbf{w}\|_2^2$. In group lasso, sparse group lasso, overlapping group lasso, the regularization term requires to divide \mathbf{w} into different overlapping or non-overlapping groups. The partition of \mathbf{w} into overlapping or non-overlapping groups is often determined by properties of X .

In this paper, we propose a novel sparse range-constrained learning (SRCL) algorithm for medical image grading using a

newly introduced range constraint regularization term. Different from most of existing sparse learning algorithms, SRCL integrates the final objective of grading the medical images with the objective of finding a sparse representation into one function and solves the problem in one step. The method is able to find a sparse representation of the image based on images that are similar to the testing image in both the data or feature representation and the medical grading scores. We then apply the new proposed SRCL to two different applications for CDR computation and cataract grading.

Contribution: Our main contributions are summarized as follows.

- 1) We propose a new regularization term named range constraint to regularize the computation of the grades of medical images.
- 2) By combining the proposed range constraint with the objective of sparse learning, we propose a novel SRCL method for medical image grading. It integrates the objective of grading the medical images with the objective of finding a sparse representation into one function.
- 3) The proposed SRCL algorithm is applied to two different applications including CDR computation and cataract grading. Experimental results show that the proposed methods improve the accuracy in CDR computation and cataract grading.
- 4) The method is a general approach and can be extended for other medical image grading applications.

The rest of the paper is organized as follows. In section II, we introduce the related work. In section III, we introduce the proposed SRCL algorithm including the formulation of SRCL and its solution. Section IV shows the use of SRCL for CDR computation and cataract grading. Section V show the experimental results, followed by the discussions and conclusions in the last section.

II. RELATED WORK

Recently, sparse learning methods have begun to be used for medical image grading, such as CDR computation from retinal fundus images [22], [37], [38] and cataract grading from slit-lamp lens images [21]. These sparse learning methods compute the grade of medical images in two steps. The first step is to reconstruct the testing images based on a set of reference images. The second step is to compute the grade based on the reconstruction coefficients. Here we briefly introduce these methods and discuss their limitations.

A. Reconstruction of images

Different constraints are used to regularize the selection of atoms from the overcomplete dictionary to reconstruct the testing data \mathbf{y} in the first step. In [37], locality-constrained linear coding (LLC) [29] was used to reconstruct the disc image:

$$\min_{\mathbf{w}} \|\mathbf{y} - X\mathbf{w}\|_2^2 + \lambda_1 \|\mathbf{c} \odot \mathbf{w}\|_2^2, \quad (5)$$

where $\mathbf{c} = [c_1, c_2, \dots, c_n]^T \in \mathbb{R}^n$ and $c_i = \exp(-\frac{\|\mathbf{y} - \mathbf{x}_i\|_2^2}{2\sigma^2})$ denotes the Gaussian distance between \mathbf{x}_i and \mathbf{y} . The limitation of the approach is that the solution is not sparse. In addition,

the pixel-wise distance between two disc images suffers from various noise including blood vessels, disc alignment error, etc. This method has also been used to reconstruct cataract images for cataract grading [39].

In sparse coding (SC) [40], ℓ_1 norm regularization is added into the objective function to get a sparse solution:

$$\min_{\mathbf{w}} \|\mathbf{y} - X\mathbf{w}\|_2^2 + \lambda_1 \|\mathbf{w}\|_1. \quad (6)$$

However, the basic form of SC approach is not optimized for specific applications such as CDR estimation. Inspired by the idea that discs with similar CDRs shall be similar in shape and the idea of a few similar discs shall be sufficient for CDR estimation, sparse dissimilarity-constrained coding (SDC) has been proposed [22]:

$$\min_{\mathbf{w}} \|\mathbf{y} - X\mathbf{w}\|_2^2 + \lambda_1 \|\mathbf{w}\|_1 + \lambda_2 \|\mathbf{d} \odot \mathbf{w}\|_2^2, \quad (7)$$

where $\mathbf{d} = [d_1, d_2, \dots, d_n]^T \in \mathbb{R}^n$ and d_i denotes the similarity based distance between \mathbf{x}_i and \mathbf{y} . Compared with LLC, SDC includes the ℓ_1 norm constraint to yield a sparse solution. In addition, a new distance \mathbf{d} based on the similarity of the discs is proposed. SDC leads to sparse solution with higher weights in discs similar to the testing images, however, it may reconstruct the testing disc image using discs with quite different CDR values. This is not optimal for CDR computation in the next step.

In [38], the reference disc images have been divided into non-overlapping groups based on their CDR values and group sparsity has been included into the objective function:

$$\min_{\mathbf{w}} \|\mathbf{y} - X\mathbf{w}\|_2^2 + \lambda_1 \|\mathbf{w}\|_1 + \lambda_2 \|\mathbf{d} \odot \mathbf{w}\|_2^2 + \lambda_3 \sum_{i=1}^N \psi_i \|\mathbf{w}_{G_i}\|_2, \quad (8)$$

where \mathbf{w} is divided into N non-overlapping groups $\mathbf{w}_{G_1}, \mathbf{w}_{G_2}, \dots, \mathbf{w}_{G_N}$, ψ_i controls the weight of i^{th} group, λ_3 controls the weight of the overall group lasso term. Although the sparse group sparsity leads to a sparse solution from each group, several groups with quite different CDRs may still be used.

B. Grade computation

After solving \mathbf{w} based on different objective functions above, the grade \hat{g} of the testing image is then computed in the second step [22]:

$$\hat{g} = \frac{1}{\mathbf{1}^T \mathbf{w}} \mathbf{w}^T \mathbf{g}, \quad (9)$$

where $\mathbf{1}$ is a vector of 1s with length n , $\mathbf{g} = [g_1, g_2, \dots, g_n]^T \in \mathbb{R}^n$, g_i denotes the grades for \mathbf{x}_i .

It has been assumed that the minimization of the objective function in the first step will lead to a better estimation of the grade in the second step. However, this is not necessarily true. In fact, in the first step to find the representation of the data, the regularization constraint is computed from the data \mathbf{y} and the atoms in the dictionary X only. The grade \mathbf{g} of the atoms in the dictionary X has not been considered. In another word, the first step to reconstruct the images is independent from the

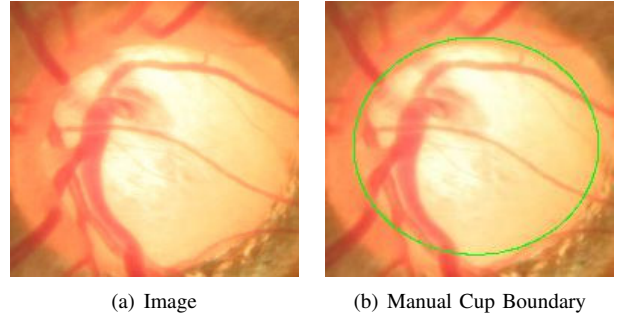


Fig. 2. An example of optic disc image: green line indicates the manual cup boundary, from which the CDR value of 0.79 is computed. The disc image is processed to be the input vector \mathbf{y} for sparse learning reconstruction.

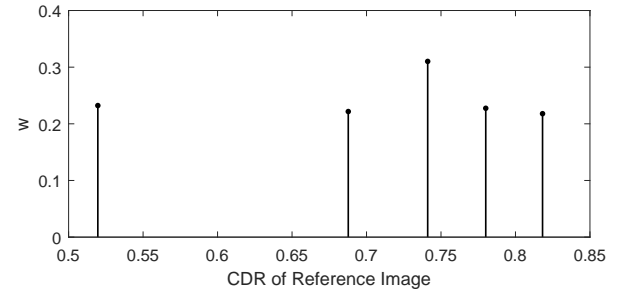


Fig. 3. Illustration of sparse coding in medical image grading: top five coefficients in \mathbf{w} are plotted.

second step to compute the grading score. The objective in the first step is not necessarily optimized for the second step.

We use an actual case as an example and the SC [40] algorithm is used to reconstruct the retinal image in Fig. 2(a). In SC, we compute \mathbf{w} based on (6). For simplicity, we plot the top five coefficients in \mathbf{w} and the CDRs of the corresponding discs. As shown in Fig. 3, the five discs corresponding to the top five coefficients have CDRs of 0.74, 0.51, 0.78, 0.68 and 0.81. The second disc has a CDR of 0.51, much lower than other discs. This leads to challenges in estimate \hat{g} . One would ask for the reason that a disc with obviously lower CDR of 0.51 can have a high weight in \mathbf{w} . This is actually because the data term is not perfect and it is corrupted by many factors, e.g., retinal vessels, error in disc segmentation, un-even illumination across the disc, etc.

It should be noted that the above bias might also be caused by the linear image grading computation in (9), which is actually an approximation of actual grading score. To explain this, we artificially create a disc image $\hat{\mathbf{y}} = \frac{1}{2}(\mathbf{x}_1 + \mathbf{x}_2)$ and its ideal reconstruction $\hat{\mathbf{w}}$ with two non-zero values $\hat{w}_1 = \hat{w}_2 = 0.5$ and $\hat{w}_i = 0, \forall i \geq 3$. Based on equation (9), the computed CDR would be $\frac{1}{2}(g_1 + g_2)$. However, the manual CDR of $\hat{\mathbf{y}}$ depends on the summation of \mathbf{x}_1 and \mathbf{x}_2 and may not be $\frac{1}{2}(g_1 + g_2)$. The difference in between can be large if $|g_1 - g_2|$ is large.

III. SPARSE RANGE-CONSTRAINED LEARNING

Since the objective of our reconstruction is to compute the grading of \mathbf{y} , intuitively, we intend to have high weights for atoms with similar grades and low or even zero weights for

those with quite different grades. Ideally, we want to find a subset ϕ of the atoms whose grades satisfy:

$$|\hat{g} - g_m| < \epsilon, \forall \mathbf{x}_m \in \phi \quad (10)$$

where \hat{g} denotes the grade of \mathbf{y} , g_m denotes the grade of \mathbf{x}_m in ϕ and ϵ is a small positive value.

A. Range constraint

Inspired from the above discussions, we propose a new constraint to use atoms that have grading scores close to the testing image. In another word, we want to find a subset of atoms $\{\mathbf{x}_i\}, i \in \{1, 2, \dots, n\}$, whose grades g_i are close to that of the testing image. Therefore, we want to minimize $|\hat{g} - g_i|$ for entries with non-zero weights w_i . The proposed range constraint (RC) term is defined as:

$$\sum_i (w_i(\hat{g} - g_i))^2 \quad (11)$$

We name the proposed constraint term as range constraint because it tends to reduce the range $\max_{p,q} |g_p - g_q|$ with non-zero w_p and w_q . The matrix form of the RC term is given as

$$\|\mathbf{w} \odot (\hat{\mathbf{g}} - \mathbf{g})\|_2^2, \quad (12)$$

where $\hat{\mathbf{g}}$ is a vector of \hat{g} with length n . Intuitively, an atom \mathbf{x}_i shall have a low or even zero weight w_i if $|\hat{g} - g_i|$ is large. Different from previous regularization terms which are functions of \mathbf{w} , RC is a function of both \mathbf{w} and $\hat{\mathbf{g}}$.

B. Formulation of SRCL

As we mentioned earlier, a limitation of previous sparse learning based algorithms for medical image grading is that the step of reconstructing the testing images from the reference is independent from the step of computing the grades. To overcome this limitation, we propose to integrate the above RC term with the data term $\|\mathbf{y} - X\mathbf{w}\|_2^2$ and the regularization term $r(\mathbf{w})$. The general objective function for SRCL is given by:

$$\min_{\mathbf{w}, \hat{\mathbf{g}}} \|\mathbf{y} - X\mathbf{w}\|_2^2 + \lambda \cdot r(\mathbf{w}) + \gamma \cdot \|\mathbf{w} \odot (\hat{\mathbf{g}} - \mathbf{g})\|_2^2, \quad (13)$$

where γ controls the weight of RC term.

Different from previous methods [40], [22], [41], SRCL considers both \mathbf{w} and $\hat{\mathbf{g}}$ in the objective function. This function is general and can be combined with different forms of $r(\mathbf{w})$. The benefits of new regularizer are twofold. On the one hand, by integrating this term into the objective function, we can solve \mathbf{w} and $\hat{\mathbf{g}}$ simultaneously in one step. On the second hand, it also affects the solution of \mathbf{w} . More specifically, the new term leads to a solution \mathbf{w} such that w_i is non-zero only for a small number of atoms with very close grades. This helps to reduce the bias as we have discussed in Section II. Below, we show how to solve \mathbf{w} and $\hat{\mathbf{g}}$.

C. Solution of SRCL

Since we have two unknowns \mathbf{w} and $\hat{\mathbf{g}}$ in (13), we solve them by alternatively solving the two subproblems below until convergence:

$$\min_{\mathbf{w}_t} \|\mathbf{y} - X\mathbf{w}_t\|_2^2 + \lambda \cdot r(\mathbf{w}_t) + \gamma \cdot \|\mathbf{w}_t \odot (\hat{\mathbf{g}}_{t-1} - \mathbf{g})\|_2^2, \quad (14)$$

$$\min_{\hat{\mathbf{g}}_t} \|\mathbf{y} - X\mathbf{w}_t\|_2^2 + \lambda \cdot r(\mathbf{w}_t) + \gamma \cdot \|\mathbf{w}_t \odot (\hat{\mathbf{g}}_t - \mathbf{g})\|_2^2. \quad (15)$$

To solve the first subproblem in (14), we rewrite it as:

$$\begin{aligned} & \min_{\mathbf{w}_t} \|\mathbf{y} - X\mathbf{w}_t\|_2^2 + \lambda \cdot r(\mathbf{w}_t) + \gamma \cdot \|\mathbf{w}_t \odot (\hat{\mathbf{g}}_{t-1} - \mathbf{g})\|_2^2 \\ & = \min_{\mathbf{w}_t} \left\| \begin{bmatrix} \mathbf{y} \\ \mathbf{0} \end{bmatrix} - \begin{bmatrix} X \\ \sqrt{\gamma}\Delta \end{bmatrix} \mathbf{w}_t \right\|_2^2 + \lambda \cdot r(\mathbf{w}_t) \\ & = \min_{\mathbf{w}_t} \|\hat{\mathbf{y}} - \hat{X}\mathbf{w}_t\|_2^2 + \lambda \cdot r(\mathbf{w}_t), \end{aligned} \quad (16)$$

where $\hat{\mathbf{y}} = \begin{bmatrix} \mathbf{y} \\ \mathbf{0} \end{bmatrix} \in \mathbb{R}^{m+n}$, $\mathbf{0}$ is a vector of 0s with length n , $\hat{X} = \begin{bmatrix} X \\ \sqrt{\gamma}\Delta \end{bmatrix} \in \mathbb{R}^{(m+n) \times n}$ and $\Delta \in \mathbb{R}^{n \times n}$ denotes a diagonal matrix with $\Delta(i, i) = \hat{g}_{t-1} - g_i$. This implies that we can always integrate the RC with the data term and solve the subproblem in (14) as the original problem without the range constraint.

The second subproblem in (15) has a closed-form solution. Since $\hat{\mathbf{g}}_t$ is a vector of \hat{g}_t with length n , we compute the first derivative of the term with respect to \hat{g}_t . By letting the first derivative of the term to be zero, it is easy to find out that

$$\hat{g}_t = \frac{\sum_{i=1}^n w_i^2 g_i}{\sum_{i=1}^n w_i^2} \quad (17)$$

We iteratively solve the above two subproblems until convergence or the maximum number of iteration arrives.

It can be seen that:

$$\hat{g}_t = \frac{\sum_{i=1}^n w_i^2 g_i}{\sum_{i=1}^n w_i^2} \leq \frac{\sum_{i=1}^n w_i^2 g_{max}}{\sum_{i=1}^n w_i^2} = g_{max}, \quad (18)$$

where $g_{max} = \max\{g_1, g_2, \dots, g_n\}$ denotes the maximum value of $g_i, i = 1, 2, \dots, n$.

Similarly, it can also be proved that $\hat{g}_t \geq g_{min}$ and g_{min} denotes the minimum value of $g_i, i = 1, 2, \dots, n$. Since $g_{min} \leq \hat{g}_t \leq g_{max}$ in each iteration, the final computed grades will also be in the range of $[g_{min} \ g_{max}]$. Therefore, the computed \hat{g} is always in the same scale range of that for the dictionary images.

Depending on the regularization term $r(\mathbf{w})$, we may solve the subproblem in (14) differently. Below, we discuss the three different forms of SRCL algorithms based on different $r(\mathbf{w})$ from SC, SDC and SSGL. By combining the RC with these methods, we obtain three different SRCL methods in this paper, denoted as SC+RC, SDC+RC and SSGL+RC.

1) SC+RC:

$$r(\mathbf{w}) = \frac{\lambda_1}{\lambda} \|\mathbf{w}\|_1. \quad (19)$$

In this situation, we use the objective function $r(\mathbf{w})$ as that of SC [40]:

$$\begin{aligned} f(\mathbf{w}_t) & = \|\mathbf{y} - X\mathbf{w}_t\|_2^2 + \lambda_1 \cdot \|\mathbf{w}_t\|_1 + \gamma \|\mathbf{w}_t \odot (\hat{\mathbf{g}}_{t-1} - \mathbf{g})\|_2^2 \\ & = \|\hat{\mathbf{y}} - \hat{X}\mathbf{w}_t\|_2^2 + \lambda_1 \cdot \|\mathbf{w}_t\|_1. \end{aligned} \quad (20)$$

Since $f(\mathbf{w}_t)$ integrates SC with RC, we denote the approach as ‘‘SC+RC’’. Minimization of (20) is a standard ℓ_1 -norm regularized least square minimization problem. It has been shown that this unconstrained convex optimization problem can be solved by least angle regression (LARS) [42].

2) *SDC+RC*:

$$r(\mathbf{w}) = \frac{\lambda_1}{\lambda} \|\mathbf{w}\|_1 + \frac{\lambda_2}{\lambda} \|\mathbf{d} \odot \mathbf{w}\|_2^2. \quad (21)$$

In this situation, we use the objective function $r(\mathbf{w})$ as that of SDC [22]. Therefore we denote this approach as ‘‘SDC+RC’’. It shall be noted that the ‘distance’ here can be computed by any form, such as dissimilarity or other distance between \mathbf{x}_i and \mathbf{y} . We have:

$$f(\mathbf{w}_t) = \|\hat{\mathbf{y}} - \hat{X}\mathbf{w}_t\|_2^2 + \lambda_1 \|\mathbf{w}_t\|_1 + \lambda_2 \|\mathbf{d} \odot \mathbf{w}_t\|_2^2. \quad (22)$$

It has been shown in [22] that the third term in (22) can be merged into the first term. Therefore, ‘‘SDC+RC’’ is still a ℓ_1 -norm regularized least square minimization problem that can be solved by LARS.

3) *SSGL+RC*:

$$r(\mathbf{w}) = \frac{\lambda_1}{\lambda} \cdot \|\mathbf{w}\|_1 + \frac{\lambda_2}{\lambda} \|\mathbf{d} \odot \mathbf{w}\|_2^2 + \frac{\lambda_3}{\lambda} \cdot \sum_{i=1}^N \psi_i \|\mathbf{w}_{G_i}\|_2. \quad (23)$$

In this situation, we use the objective function $r(\mathbf{w})$ as that of SSGL [38] and the approach is therefore denoted as ‘‘SSGL+RC’’. Similarly, we have:

$$f(\mathbf{w}_t) = \|\hat{\mathbf{y}} - \hat{X}\mathbf{w}_t\|_2^2 + \lambda_1 \|\mathbf{w}_t\|_1 + \lambda_2 \|\mathbf{d} \odot \mathbf{w}_t\|_2^2 + \lambda_3 \sum_{i=1}^N \psi_i \|\mathbf{w}_{t_{G_i}}\|_2. \quad (24)$$

As illustrated in [38], minimizing the objective function in (24) can be converted to a standard sparse group lasso problem. We solve the problem using the sparse learning with efficient projection (SLEP) package [43].

In this paper, we mainly discuss the above three forms of $r(\mathbf{w})$. We leave it to the respective readers to find the applications of other regularization terms.

IV. SRCL FOR MEDICAL IMAGE GRADING

In this section, we show the use of SRCL for two different medical image grading applications: CDR computation from retinal fundus images and cataract grading from slit-lamp lens images.

A. Cup-to-disc ratio computation

The first application is to compute the CDR from retinal fundus images. CDR is often computed as the ratio of vertical cup diameter to vertical disc diameter. It is a commonly used indicator in glaucoma detection. A higher CDR often indicates a higher risk of glaucoma. Previously, SC [40], SDC [22] and SSGL [38] have been proposed for CDR computation. In SDC and SSGL, the distance \mathbf{d} is computed based on the shape similarity of the disc images as in [22].

In this paper, we use all the three previous approaches SC, SDC and SSGL as baselines to show how the RC term

improves the CDR computation. As showed in Section III-C, by adding the RC term into the objective function of SC, SDC and SSGL, we have three new algorithms denoted as SC+RC, SDC+RC and SSGL+RC, respectively. Recall that in Section III-C, we solve \mathbf{w}_t and \hat{g}_t iteratively. We need to obtain an initial grade \hat{g}_0 to compute \mathbf{w}_1 . For SC+RC, SDC+RC and SSGL+RC, we use the results from SC, SDC and SSGL as the initial values for \hat{g}_0 , respectively. CDR is obtained after solving the problems in (14) and (15) iteratively.

B. Cataract grading

Cataracts are the leading cause of blindness worldwide. Cataract grading is essential for diagnosis and progression monitoring of the disease. In cataract grading, the images are first graded with decimal grading scores that range from 0.3 to 5.0 by professional graders based on the Wisconsin protocol [44]. The protocol takes the ceiling of each decimal grading score as the integral grading score. In our grading, we use the decimal grading scores before the ceiling as the ground truth scores. Similar to CDR computation, we also use SC, SDC and SSGL as the baselines. Therefore we have SC+RC, SDC+RC and SSGL+RC for cataract grading as well. Following the method in [21], the distance d_i is computed as χ^2 -distance between the testing image \mathbf{y} and the reference image \mathbf{x}_i for SDC, SSGL, SDC+RC and SSGL+RC. Similar to that in CDR computation, we also use SC, SDC and SSGL to get initial grades for SC+RC, SDC+RC and SSGL+RC, respectively.

A decimal score is obtained for cataract grading by solving the problems in (14) and (15) iteratively. A ceiling operation is further applied to get the integral grading score.

V. EXPERIMENTAL RESULTS

A. Cup-to-disc ratio computation

1) *Data Set*: We use 650 images from ORIGA data set [45]. The data set consists of 168 images from glaucomatous eyes and 482 images from randomly selected normal eyes from a population based study. The ground truth CDR is computed as the ratio of vertical cup diameter to vertical disc diameter from optic cup and optic disc boundaries manually labelled by trained professionals. The images are partitioned into two subsets A and B previously and we followed the same partition in this paper [38]. In our experiments, we use images from set A as reference or training images and images from set B as testing images. Since different disc images have different dimensions, we resize all the images to the same size. Following that in [22], we resize all disc images to 50×50 pixels for less computational cost.

2) *Evaluation Metrics*: The following criteria are used in our evaluation:

- mean absolute CDR error:

$$\delta = \frac{1}{N} \sum_i^N |GT_i - CDR_i|, \quad (25)$$

where GT_i and CDR_i denote the manually and automatically measured CDR of sample i , N denotes the number of testing images.

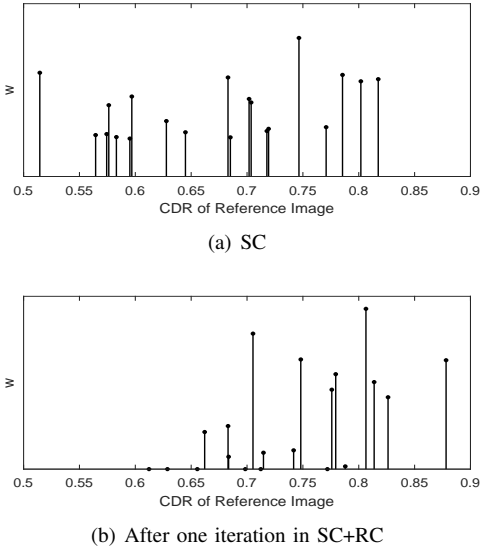


Fig. 4. Top 20 non-zero elements in \mathbf{w} when reconstruct an image using SC and SC+RC.

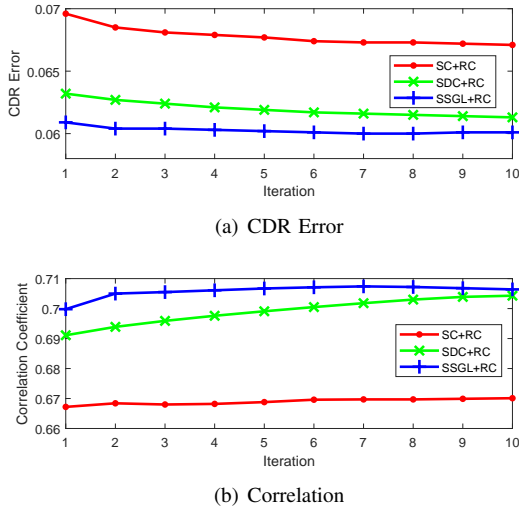


Fig. 5. Performance changes during the iteration of SC+RC, SDC+RC and SSGL+RC.

- The correlation: the Pearson's correlation coefficient between the manually measured CDRs and automatically computed CDRs is computed.

3) *Results*: To show how the RC term affects the results, we first look at how the parameter \mathbf{w}_t changes as t iterates. We take the SC+RC as an example. Fig. 4 shows the top 20 non-zero elements in \mathbf{w}_t before and after the first iteration for the disc in Fig. 2 with manual CDR of 0.79. In the figure, x -axis indicates the CDR value of the images with non-zeros weights from the dictionary X and y -axis indicates the corresponding weight in \mathbf{w}_t for these images. From the figure, we can see that the elements with top 20 non-zero weights are have a wide range of CDR values from 0.51 to 0.82. After one iteration, the elements with top 20 non-zero weights have a smaller range of CDR values from 0.67 to 0.86. Correspondingly, the computed CDR values before and after the iteration are 0.68 and 0.77 respectively. Further iterations continue to reduce the range.

Fig. 5 shows the mean CDR errors and the correlation coefficients with respect to manual ground truth by SC+RC, SDC+RC and SSGL+RC for t from 1 to 10 computed from all 325 testing images in set B . The results shows that, by integrating RC into the objective function, we are able to obtain more accurate CDR values and higher correlations. It is also observed that SC+RC, SDC+RC and SSGL+RC converges with different speed. SSGL+RC converges fastest after 4 to 5 iterations. SDC+RC requires around 8 iterations and SC+RC requires more iterations to converge.

In Fig. 6, we show sample results from two images with different CDRs as well as the reconstruction coefficients by SDC and SDC+RC methods. In Fig. 7, we show the results by SSGL and SSGL+RC methods. As we can see, by including the RC term into SDC and SSGL, we reduce the CDR range of discs with non-zero reconstruction coefficients and obtain more accurate results. A limitation of SRCL is that the computational cost increases linearly depending on the number of iterations. Based on our MATLAB implementations in a dual core 2.1 GHz PC with 128 GB RAM, it takes 0.27 and 0.28 second to compute an initial grade using SC and SDC method respectively. Each iteration of computing w_t and \hat{g}_t takes 0.13 second on average for both SC+RC and SDC+RC methods. For SSGL+RC, it takes 0.16 second to compute an initial grade and each iteration requires 0.035 second on average using the same PC.

Table I compares the results with different methods. For simplicity, we use $t = 5, 8, 10$ for SSGL+RC, SDC+RC, SC+RC, respectively. We have also conducted a comparison with the state-of-the-art segmentation based approaches. Three methods are compared, including the superpixel classification [46], the U-Net deep learning [47] and the latest M-Net deep learning [48]. To have a fair comparison, the same sets of training and testing images are used. In addition, the original implementations are used to get the results. From the results, we can see that the SRCL based method outperforms the segmentation based methods.

Noted that there are several parameters λ_1 , λ_2 , λ_3 and γ in these methods. A cross-validation within the reference set has been conducted to determine λ_1 , λ_2 , λ_3 in [22], [38]. We use the same settings: For SC, SC+RC, SDC and SDC+RC, λ_1 does not need a manually determined value. As discussed in the paper, they are essentially the same the standard ℓ_1 -norm regularized least square minimization problem, which is solved using LARS [42]. In LARS, this problem is converted into the following constrained optimization problem:

$$\arg \min_w (\|\hat{\mathbf{y}} - \hat{X}\mathbf{w}\|^2), s.t., \|\mathbf{w}\|_1 < s, \quad (26)$$

where s is inversely related to λ_1 . Both s and \mathbf{w} are updated iteratively in the LARS. Previous experience [22] shows that an iteration of 100 time (i.e. $s = 100$) in LARS is able to obtain a good result and this paper uses 100 iterations for all the ℓ_1 -norm regularized least square minimization problem. For SDC and SDC+RC, λ_2 is set as 10^4 . In SSGL and SSGL+RC, we set $\lambda_1=0.01$, $\lambda_2=10$ and $\lambda_3=0.05$. γ is a new parameter to control the weight of the RC term. In SC+RC and SDC+RC, $\gamma=200$. In SSGL+RC, $\gamma=100$. Our experience

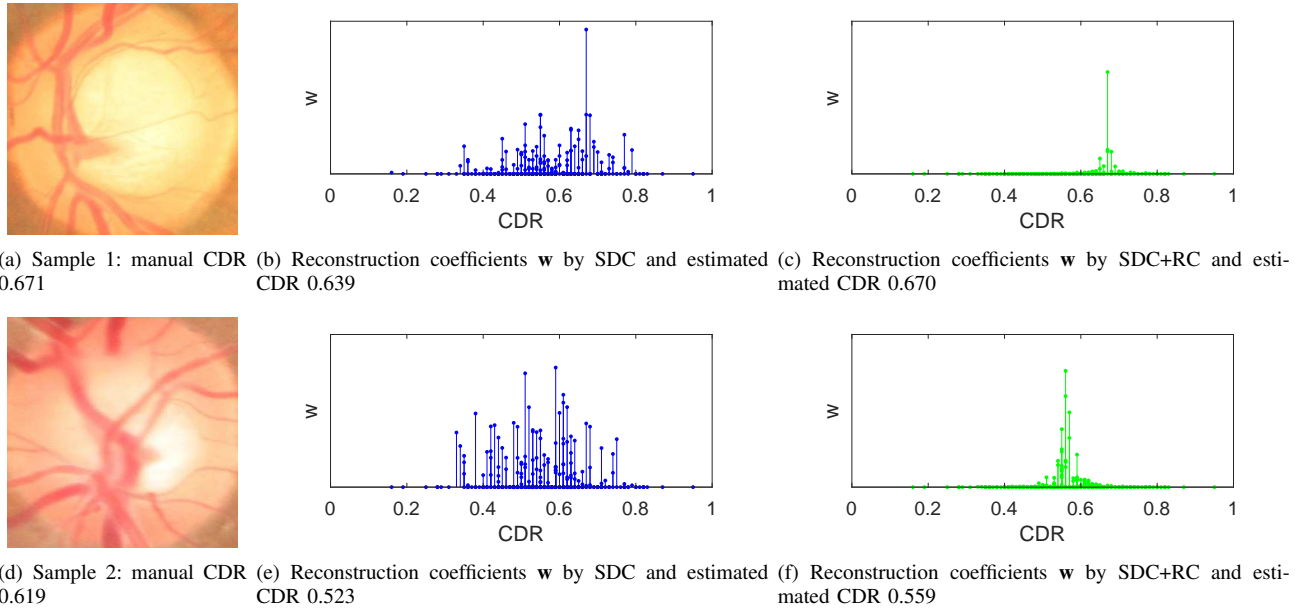


Fig. 6. Samples images with reconstruction coefficients w and resultant CDRs by SDC and SDC+RC methods.

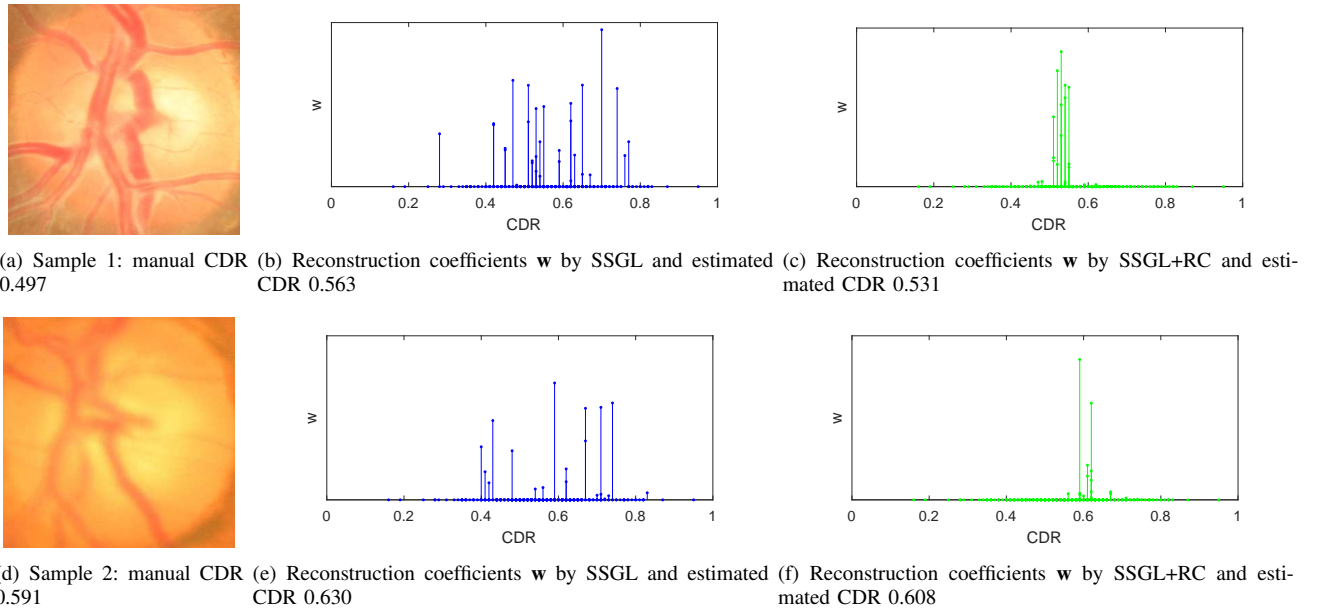


Fig. 7. Samples images with reconstruction coefficients w and resultant CDRs by SSGL and SSGL+RC methods.

shows that a small change of the parameters does not affect much the results.

B. Cataract grading

1) *Dataset*: We use the ACHIKO-NC dataset [49]. It has 5378 images with both decimal grading score based on Wisconsin protocol [44]. By taking the ceiling of the decimal scores, ACHIKO-NC has 94 images of integral score 1, 1874 images of integral score 2, 2476 images of integral score 3, 897 images of integral score 4 and 37 images of integral score 5. In the experiments, we use the decimal score as manual ground truth in the calculation.

TABLE I
PERFORMANCE COMPARISON OF SRCL FOR CDR COMPUTATION.

	CDR Error	Correlation
Superpixel [46]	0.0774	0.590
U-net [47]	0.0740	0.532
M-net [48]	0.0710	0.586
SC [40]	0.0696	0.667
SDC [22]	0.0660	0.686
SSGL [38]	0.0616	0.700
SC+RC	0.0669	0.671
SDC + RC	0.0613	0.704
SSGL +RC	0.0599	0.708

2) *Evaluation Metrics*: Following the previous work [49], we use four evaluation criteria to measure the grading accuracy:

- ϵ : the mean absolute error

$$\epsilon = \frac{1}{N} \sum |G_i - M_i| \quad (27)$$

- R_0 : the integral agreement ratio

$$R_0 = \frac{1}{N} \|\lceil G_i \rceil = \lceil M_i \rceil\|_0 \quad (28)$$

- $R_{0.5}$: the percentage of decimal grading with error ≤ 0.5

$$R_{0.5} = \frac{1}{N} \|\lceil G_i \rceil - \lceil M_i \rceil \leq 0.5\|_0 \quad (29)$$

- R_1 : the percentage of decimal grading with error ≤ 1

$$R_1 = \frac{1}{N} \|\lceil G_i \rceil - \lceil M_i \rceil \leq 1\|_0 \quad (30)$$

Here G_i denotes the automatically computed grade for the i^{th} image, and M_i denotes manual ground truth grade, $\lceil \cdot \rceil$ denotes the ceiling function, $\|\cdot\|_0$ denotes the ℓ_0 norm.

In cataract grading, the lens is first detected by the active shape model [49] and divided into three parts including the nucleus part, anterior cortex part and posterior cortex part. The bag-of-words (BoW) model [50] is used to extract features from the three different parts. The BoW model provides a location-independent global representation of local features which are invariant to rotation, scaling or affine transform. In cataract grading, the local features in our BoW model are image patches that represent intensity and texture information. Each part of the resized lens image is divided into a grid of half-overlapping $s \times s$ patches and $s = 3$ in our experiments. After obtaining all the local patches from a set of training images, k -means clustering technique is applied to generate the codebook from randomly selected samples, and then the BoW is computed from a binning procedure, where the clustering parameter k is referred to as the bin number. More details of BoW computation can be found in [50].

We use a randomly selected 340 images as reference data, where the number of images from grade 1 to 5 are 20, 100, 100, 100, 20 respectively. We use fewer images from grade 1 and 5 because the number of images in these two grades are much smaller than other grades. The remaining 5038 images are used for testing. Similar to that in CDR computation, we integrate RC with SC, SDC and SSGL to get the results by SC+RC, SDC+RC and SSGL+RC. A cross-validation within the reference set is conducted to determine the parameters. Similarly, λ_1 does not need to be determined in LARS for SC, SDC, SC+RC, SDC+RC. For SDC and SDC+RC, we set $\lambda_2=2$. For SSGL and SSGL+RC, $\lambda_1=0.035, \lambda_2=10, \lambda_3=0.05$. The new parameter $\gamma=100$ in all the experiments. The results are summarized in Table II. In addition, we have also compared the proposed method with other methods. Two algorithms are compared, including the RBF kernel-based support vector regression (RBF+SVR) approach [49] and group lasso regression approach (GSR) [21]. As we can see, the proposed method outperforms other methods. In Fig. 8, we also plot the automatic grading by SSGL+RC against that of a professional grader, which demonstrates that the proposed method has good agreement with the professional grader.

TABLE II
PERFORMANCE COMPARISON OF SRCL FOR CATARACT GRADING.

	ϵ	R_0	$R_{0.5}$	R_1
RBF+SVR [49]	0.363	0.615	0.711	0.980
BoW+GSR [21]	0.356	0.679	0.750	0.983
LLC [39]	0.331	0.688	0.767	0.987
SC [40]	0.367	0.666	0.724	0.980
SDC [22]	0.350	0.681	0.741	0.986
SSGL [38]	0.339	0.677	0.758	0.986
SC+RC	0.329	0.687	0.761	0.987
SDC + RC	0.325	0.691	0.771	0.988
SSGL+RC	0.322	0.691	0.780	0.989

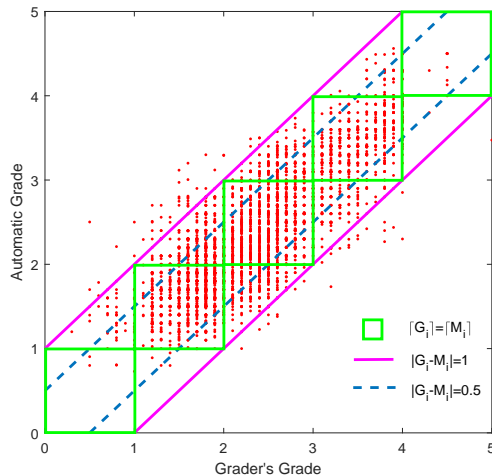


Fig. 8. Visual illustration of the agreement between automatic grading by SSGL+RC and the Grader's grading.

VI. DISCUSSIONS AND CONCLUSIONS

In this paper, we propose a new regularization term named range constraint and combine it with sparse learning for SRCL. The proposed SRCL is able to improve the automatic grading of CDR from retinal fundus images and cataract severity from slit-lamp lens images. Here we discuss a little more why it works and how we can extend it for other applications. Recall that in the grading, we want to find some atoms from the dictionary to reconstruct a testing image \mathbf{y} . However, there is no perfect data representation (either the original image representation or a feature map computed from the image), such that a distance d computed from the data perfectly reflects the grading of the image. Therefore, some atoms may have high weights in \mathbf{w} , though they are not really similar to \mathbf{y} in the grading. By introducing the range-constraint, we avoid to reconstruct the testing images with atoms that have quite different grades.

The method can be extended for other medical image grading applications and generic image classification or grading problems. In general, it is suitable for a grading problem which aims to find a decimal score for a new image based on a set of atoms with known scores. The data representation can be from pixel intensities of the images or feature maps computed from the images. But the intensities or the feature maps shall have the property that those images similar in the grading

scores shall be similar in the data representation. Therefore, we need to find appropriate data representation when applying the model to other grading problems for medical or generic images. A potential application is the age estimation from facial images. To make the algorithm applicable for age estimation, one needs to compute a feature representation of the images such that the features of images from similar ages are often close. We will explore the use of the algorithm for such application in future work. It should be noted that for a grading problem without decimal scores as ground truth, SRCL may not have much advantages as the rounding error may be introduced to the grading.

In this paper, we propose a novel sparse range-constrained learning method for medical image grading. It combines the objective of sparse learning with the objective of medical image grading into one function. Our results show that such a combination is effective and leads to better performance in both CDR computation and cataract grading. Our method is a general approach and it can be extended for automatic grading of other diseases. A limitation of our approach is that it requires more computational cost. A second limitation is that the method is not applicable for a problem that cannot be solved well by a sparse coding based method. Noise will also affect the performance of the method. In case of applications where the images have moderate or high level of noise, we may need to develop or apply some algorithms to remove the noise before or during the feature extraction.

REFERENCES

- [1] K. Adiloglu, A. Annies, E. Wahlen, H. Purwins, and K. Obermayer, "A graphical representation and dissimilarity measure for basic everyday sound events," *IEEE Transactions on Audio, Speech, and Language Processing*, vol. 20, no. 5, pp. 1542–1552, 2012.
- [2] Y. Li, A. Cichocki, and S. Amari, "Analysis of sparse representation and blind source separation," *Neural Computation*, vol. 16, no. 6, pp. 1193–1234, 2004.
- [3] M. Maggioni, V. Katkovnik, K. Egiazarian, and A. Foi, "Nonlocal transform-domain filter for volumetric data denoising and reconstruction," *Image Processing, IEEE Transactions on*, vol. 22, no. 1, pp. 119–133, 2013.
- [4] L. Fang, S. Li, R. P. McNabb, Q. Nie, A. N. Kuo, C. A. Toth, J. A. Izatt, and S. Farsiu, "Fast acquisition and reconstruction of optical coherence tomography images via sparse representation," *IEEE Trans. on Medical Imaging*, vol. 32, pp. 2034–2049, 2013.
- [5] L. Fang, S. Li, Q. Nie, J. A. Izatt, C. A. Toth, and S. Farsiu, "Sparsity based denoising of spectral domain optical coherence tomography images," *Biomedical optics express*, vol. 3, pp. 927–942, 2012.
- [6] M. Elad and M. Aharon, "Image denoising via sparse and redundant representations over learned dictionaries," *IEEE Trans. on Image Processing*, vol. 15, pp. 3736–3745, 2006.
- [7] R. Kafieh, H. Rabbani, and I. Selesnick, "Three dimensional data-driven multi scale atomic representation of optical coherence tomography," *IEEE Transactions on Medical Imaging*, vol. 34, no. 5, pp. 1042–1062, 2015.
- [8] J. Cheng, L. Duan, D. W. K. Wong, D. Tao, M. Akiba, and J. Liu, "Speckle reduction in optical coherence tomography by image registration and matrix completion," *P. Golland et al. (Eds.): MICCAI 2014, Part I, LNCS 8673*, pp. 162–169, 2014.
- [9] J. Cheng, D. Tao, Y. Quan, D. W. K. Wong, G. C. M. Cheung, M. Akiba, and J. Liu, "Speckle reduction in 3d optical coherence tomography of retina by a-scan reconstruction," *IEEE Transactions on Medical Imaging*, vol. 35, no. 10, pp. 2270–2279, 2016.
- [10] F. Kou, Z. Li, C. Wen, and W. Chen, "L0 smoothing based detail enhancement for fusion of differently exposed images," *2013 IEEE 8th Conference on Industrial Electronics and Applications (ICIEA)*, pp. 1398–1403, 2013.
- [11] J. Wright, A. Y. Yang, A. Ganesh, S. S. Sastry, and Y. Ma, "Robust face recognition via sparse representation," *IEEE Transactions on Pattern Analysis and Machine Intelligence*, vol. 31, no. 2, pp. 210–227, 2009.
- [12] M. Yang and L. Zhang, "Gabor feature based sparse representation for face recognition with gabor occlusion dictionary," *European Conference on Computer Vision*, pp. 448–461, 2010.
- [13] C.-Y. Lu, H. Min, J. Gui, L. Zhu, and Y.-K. Lei, "Face recognition via weighted sparse representation," *Journal of Visual Communication and Image Representation*, vol. 24, no. 2, pp. 111–116, 2013, Sparse Representations for Image and Video Analysis.
- [14] J.-X. Mi and J.-X. Liu, "Face recognition using sparse representation-based classification on k-nearest subspace," *PLOS ONE*, vol. 8, no. 3, pp. 1–11, 03 2013.
- [15] T. R. Golub, D. K. Slonim, P. Tamayo, C. Huard, M. Gaasenbeek, J. P. Mesirov, H. Coller, M. L. Loh, J. R. Downing, M. A. Caligiuri, C. D. Bloomfield, and E. S. Lander, "Molecular classification of cancer: Class discovery and class prediction by gene expression monitoring," *Science*, vol. 286, no. 5439, pp. 531–537, 1999.
- [16] Z. Zhang, Y. Xu, J. Liu, and C. K. Kwok, "Identify predictive snp groups in genome wide association study: A sparse learning approach," *Procedia Computer Science*, vol. 11, pp. 107–114, 2012.
- [17] Y. Li, G. O'Connor, D. Josee, and E. Kolaczyk, "Modeling gene-covariate interactions in sparse regression with group structure for genome-wide association studies," *Statistical Applications in Genetics and Molecular Biology*, vol. 14(3), pp. 265277, 2015.
- [18] P. Aljabar, R. A. Heckemann, A. Hammers, J. V. Hajnal, and D. Rueckert, "Multi-atlas based segmentation of brain images: Atlas selection and its effect on accuracy," *NeuroImage*, vol. 46 3, pp. 726–38, 2009.
- [19] G. Varoquaux, A. Gramfort, F. Pedregosa, V. Michel, and B. Thirion, "Multi-subject dictionary learning to segment an atlas of brain spontaneous activity," *Information Processing in Medical Imaging, Lecture Notes in Computer Science*, vol. 6801, pp. 562–573, 2011.
- [20] S. Roy, Q. He, E. Sweeney, A. Carass, D. S. Reich, J. L. Prince, and D. L. Pham, "Subject-specific sparse dictionary learning for atlas-based brain mri segmentation," *IEEE Journal of Biomedical and Health Informatics*, vol. 19, no. 5, pp. 1598–1609, 2015.
- [21] Y. Xu, X. Gao, S. Lin, D. W. K. Wong, J. Liu, D. Xu, C. Y. Cheng, C. Y. Cheung, and T. Y. Wong, "Automatic grading of nuclear cataracts from slit-lamp lens images using group sparsity regression," *In: Mori, K., Sakuma, I., Sato, Y., Barillot, C., Nassiri, N.(eds.) MICCAI 2013, Part II, LNCS*, vol. 8150, pp. 468–475, 2013.
- [22] J. Cheng, F. Yin, D. W. K. Wong, D. Tao, and J. Liu, "Sparse dissimilarity-constrained coding for glaucoma screening," *IEEE Trans. on Biom. Eng.*, vol. 62, no. 5, pp. 1395–1403, 2015.
- [23] A. M. Tillmann, "On the computational intractability of exact and approximate dictionary learning," *IEEE Signal Processing Letters*, vol. 22, no. 1, pp. 45–49, 2015.
- [24] D. L. Donoho, "For most large underdetermined systems of linear equations the minimal ℓ_1 -norm solution is also the sparsest solution," *Communications on Pure and Applied Mathematics*, vol. 59, no. 6, pp. 797–829, 2006.
- [25] J. Wright, Y. Ma, J. Mairal, G. Sapiro, T. S. Huang, and S. Yan, "Sparse representation for computer vision and pattern recognition," *Proceedings of the IEEE*, vol. 98, no. 6, pp. 1031–1044, 2010.
- [26] D. Barchiesi and M. D. Plumbley, "Learning incoherent dictionaries for sparse approximation using iterative projections and rotations," *IEEE Transactions on Signal Processing*, vol. 61, no. 8, pp. 2055–2065, 2013.
- [27] A. Argyriou, T. Evgeniou, and M. Pontil, "Convex multi-task feature learning," *Machine Learning*, vol. 73, no. 3, pp. 243–272, 2008.
- [28] R. Tibshirani, M. Saunders, S. Rosset, J. Zhu, and K. Knight, "Sparsity and smoothness via the fused lasso," *Journal Of The Royal Statistical Society Series B*, vol. 67(1), pp. 91–108, 2005.
- [29] J. Wang, J. Yang, K. Yu, F. Lv, T. Huang, and Y. Gong, "Locality-constrained linear coding for image classification," *IEEE Int. Conf. on computer vision and pattern recognition*, pp. 3360–3367, 2010.
- [30] S. Gao, I. W. H. Tsang, L. T. Chia, and P. Zhao, "Local features are not lonely-laplacian sparse coding for image classification," *2010 IEEE Computer Society Conference on Computer Vision and Pattern Recognition*, pp. 3555–3561, 2010.
- [31] S. Guo, Q. Ruan, and Z. Miao, "Similarity weighted sparse representation for classification," *Proceedings of the 21st International Conference on Pattern Recognition (ICPR2012)*, pp. 1241–1244, 2012.
- [32] J. Friedman, T. Hastie, and R. Tibshirani, "A note on the group lasso and a sparse group lasso," *Technical report, Department of Statistics, Stanford University*, 2010.

- [33] L. Jacob, G. Obozinski, and J. P. Vert, "Group lasso with overlap and graph lasso," *Proceedings of the 26th Annual International Conference on Machine Learning*, pp. 433–440, 2009.
- [34] M. J. van de Vijver, Y. D. He, L. J. van't Veer, H. Dai, A. A.M. Hart, D. W. Voskuil, G. J. Schreiber, J. L. Peterse, C. Roberts, M. J. Marton, M. Parrish, D. Atsma, A. Witteveen, A. Glas, L. Delahaye, T. van der Velde, H. Bartelink, S. Rodenhuis, E. T. Rutgers, S. H. Friend, and R. Bernards, "A gene-expression signature as a predictor of survival in breast cancer," *New England Journal of Medicine*, vol. 347, no. 25, pp. 1999–2009, 2002.
- [35] P. Zhao, G. Rocha, and B. Yu, "The composite absolute penalties family for grouped and hierarchical variable selection," *Ann. Statist.*, vol. 37(6A), pp. 3468–3497, 2009.
- [36] M. Fazel, H. Hindi, and S. P. Boyd, "A rank minimization heuristic with application to minimum order system approximation," *Proceedings of the 2001 American Control Conference. (Cat. No.01CH37148)*, vol. 6, pp. 4734–4739, 2001.
- [37] Y. Xu, S. Lin, D. W. K. Wong, J. Liu, and D. Xu, "Efficient reconstruction-based optic cup localization for glaucoma screening," *In: Mori, K., Sakuma, I., Sato, Y., Barillot, C., Nassir, N.(eds.) MICCAI 2013, Part III, LNCS*, vol. 8151, pp. 445–452, 2013.
- [38] J. Cheng, Z. Zhang, D. Tao, D. W. K. Wong, J. Liu, M. Baskaran, T. Aung, and T. Y. Wong, "Similarity regularized sparse group lasso for cup to disc ratio computation," *Biomed. Opt. Express*, vol. 8, no. 8, pp. 3763–3777, Aug 2017.
- [39] Y. Xu, L. Duan, D. W. K. Wong, T. Y. Wong, and J. Liu, "Semantic reconstruction-based nuclear cataract grading from slit-lamp lens images," *Medical Image Computing and Computer-Assisted Intervention*, pp. 458–466, 2016.
- [40] B. A. Olshausen and D. J. Field, "Emergence of simple-cell receptive field properties by learning a sparse code for natural images," *Nature*, vol. 381(6583), pp. 607–609, 1996.
- [41] N. Simon, J. Friedman, T. Hastie, and R. Tibshirani, "A sparse-group lasso," *Journal of Computational and Graphical Statistics*, vol. 22, no. 2, pp. 231–245, 2013.
- [42] B. Efron, T. Hastie, and R. Tibshirani, "Least angle regression," *Annals of Statistics*, vol. 32, pp. 68–73, 2004.
- [43] J. Liu, S. Ji, and J. Ye, *SLEP: Sparse Learning with Efficient Projections*, Arizona State University, 2009.
- [44] B. Klein, K. Klein, R. and Linton, Y. Magli, and M. Neider, "Assessment of cataracts from photographs in the beaver dam eye study," *Ophthalmology*, vol. 97, pp. 1428–1433, 1990.
- [45] Z. Zhang, F. Yin, J. Liu, D. W. K. Wong, N. M. Tan, B. H. Lee, J. Cheng, and T. Y. Wong, "Origa-light: An online retinal fundus image database for glaucoma analysis and research," *Int. Conf. of IEEE Eng. in Med. and Bio. Soc.*, pp. 3065–3068, 2010.
- [46] J. Cheng, J. Liu, Y. Xu, F. Yin, D. W. K. Wong, N. M. Tan, D. Tao, C. Y. Cheng, T. Aung, and T. Y. Wong, "Superpixel classification based optic disc and optic cup segmentation for glaucoma screening," *IEEE Trans. Med. Imaging*, vol. 32, pp. 1019–1032, 2013.
- [47] O. Ronneberger, P. Fischer, and T. Brox, "U-net: Convolutional networks for biomedical image segmentation," *Medical Image Computing and Computer-Assisted Intervention Part III*, pp. 234–241, 2015.
- [48] H. Fu, J. Cheng, Y. Xu, D. W. K. Wong, J. Liu, and X. Cao, "Joint optic disc and cup segmentation based on multi-label deep network and polar transformation," *IEEE Transactions on Medical Imaging*, vol. PP, no. 99, pp. 1–1, 2018.
- [49] H. Li, J. H. Lim, J. Liu, P. Mitchell, A. G. Tan, J. J. Wang, and T. Y. Wong, "A computer-aided diagnosis system of nuclear cataract," *IEEE Transactions on Biomedical Engineering*, vol. 57, no. 7, pp. 1690–1698, 2010.
- [50] L. Fei-Fei and P. Perona, "A bayesian hierarchical model for learning natural scene categories," *2005 IEEE Computer Society Conference on Computer Vision and Pattern Recognition (CVPR'05)*, vol. 2, pp. 524–531, 2005.